IOP Publishing Journal of Optics A: Pure and Applied Optics

J. Opt. A: Pure Appl. Opt. **11** (2009) 034009 (9pp) doi:10.1088/1464-4258/11/3/034009

Longitudinal optical binding of several spherical particles studied by the coupled dipole method

V Karásek, O Brzobohatý and P Zemánek

Institute of Scientific Instruments of the ASCR, v.v.i., Academy of Sciences of the Czech Republic, Královopolská 147, 61264 Brno, Czech Republic

E-mail: vitakar@isibrno.cz

Received 4 July 2008, accepted for publication 3 September 2008
Published 20 January 2009
Online at stacks.iop.org/JOptA/11/034009

Abstract

We employed a coupled dipole method (CDM) to study theoretically the interaction among several spherical particles placed into two counter-propagating mutually incoherent Bessel beams. This interaction is mediated by the light scattering among the particles. It has already been demonstrated that, if the intensity of the incident beam is sufficiently high, the scattered light is strong enough to self-arrange the objects in the space. Namely, the counter-propagating and incoherent Bessel beams are extremely useful to be employed because the interaction among the particles via the scattered light is not superimposed by other optical forces coming from the radiation pressure of each beam and axial gradients of the beam intensities. Therefore so-called optical binding between the particles is enhanced and leads to several stable configurations of the particles. We studied these stable configurations using the CDM for various properties of the beams and particles and we also compared these theoretical results with the experimental observations.

Keywords: optical binding, optical tweezers, optical self-arrangement, coupled dipole method, optical forces

(Some figures in this article are in colour only in the electronic version)

1. Introduction

Optical manipulation with more particles revealed that the light scattered by these particles significantly influences the equilibrium positions where the particles are confined. This interaction is called the optical binding and it results in the self-arrangement of the particles with well-defined distances between them. This phenomenon has been studied first in a lateral geometry where the particles are self-arranged in the plane perpendicular to the beam propagation. Usually an elliptical interference fringe was used to observe this so-called lateral binding experimentally on the surface [1–3]. A different configuration uses two counter-propagating incoherent beams and the particles are self-arranged along the propagation axes of the beams [4–10]. Therefore the optical binding in this configuration is called longitudinal. In both configurations the optical binding between two particles was observed if the spatial distribution of the optical intensity in the illuminating beams was almost unvarying in the direction of the particle binding. We focus here on the longitudinal binding in two counter-propagating incoherent Bessel beams because they provide an extremely long longitudinal region of unvarying spatial beam distribution. Therefore the optical interaction between the particles is not significantly superimposed by the longitudinal variation of the optical intensity of the illuminating beams and we expect longitudinal self-arrangement of particles over hundreds of micrometres. In this paper we focus especially on a detailed theoretical study of such a configuration and the results are briefly compared to the experimental observations.

Concerning the theoretical description of the optical binding several methods have already been reported. If the particles are small, they are considered as induced radiating dipoles and the interaction between them is mediated by their

radiation. Optical binding between spherical or cylindrical nanoparticles was studied in the lateral configuration [11–17] or longitudinal configuration [18]. Optical binding of larger particles was studied using the multiple Mie scattering method [19–21] or coupled dipole method (CDM) [22–24]. In this paper we have applied the CDM to study equilibrium configurations of up to five optically bound spherical particles placed into the counter-propagating incoherent Bessel beams. We found long-and short-range periodicity in the self-arranged chain of particles. We also obtained very good coincidence between the theoretical conclusions and our experimental observations and measurements.

2. Theoretical background

2.1. Description of the Bessel beam

An ideal Bessel beam is a result of an interference of the conical bunch of plane waves that all propagate with their $\boldsymbol{k}$ vectors tilted by an angle α_0 towards the optical axis z. Therefore all the plane waves have the same axial component k_z of their wavevector $\boldsymbol{k}$ and the angular spectrum of such an ideal Bessel beam is described by the delta function $\delta(\alpha - \alpha_0)$ where α is the polar angle. The interference between all plane waves results in the radial intensity distribution given by the Bessel function of the first kind and the zeroth-order $J_0(k_r\rho)$, where $\rho = \sqrt{x^2 + y^2}$ is the radial distance from the z axis and $k_r = k\sin(\alpha_0)$ is the radial component of the wavevector. The described ideal Bessel beam would propagate with unvarying lateral intensity distribution and constant on-axis intensity but also with infinite energy. In reality we can approach the properties of the ideal Bessel beam only over a limited longitudinal range. Such beams are called quasi-Bessel beams and can be obtained, for example, if a Gaussian beam passes though a conical lens (axicon). However, if the axicon is illuminated with the Gaussian beam, the plane wave spectrum behind the axicon does not have the form of the delta function. Its width increases with decreasing Gaussian beam waist w_0 [25, 26] illuminating the axicon. Such a quasi-Bessel beam still has an unvarying lateral intensity distribution shape but it exists only over a limited longitudinal range $z_{\max} = w_0\cos\alpha_0/\sin\alpha_0$. The quasi-Bessel beam can keep its unique properties over a longitudinal distance reaching hundreds of micrometres and therefore the on-axis intensity varies only slowly along the propagation axis. Therefore, for the purposes of the theoretical study of the longitudinal optical binding we can neglect this longitudinal intensity variation and we can assume that the particles move in a longitudinally unvarying field. The electric field of such a linearly polarized beam (along the x direction) can be approximated for small angles α_0 [27, 28] as

$$E_x = E_0 J_0(k_r\rho)\exp(\mathrm{i}k_z z). \tag{1}$$

For practical reasons we define the radius of the Bessel beam core ρ_0 as $J_0(k_r\rho_0) = 0$ which gives

$$\rho_0 = \frac{2.4048}{k_r} = \frac{2.4048}{k\sin(\alpha_0)}. \tag{2}$$

2.2. Calculation of optical forces and optical binding using the CDM

We modified the classical CDM algorithm for the purposes of the calculation of the optical binding between two particles [24] and especially we employed the existing symmetries in the problem to speed up the calculation. The CDM is based on the division of each object into sufficiently small domains. The volume of each domain is so small that the domain may be approximated by an induced radiating dipole. These dipoles are located at vertices of a 3D orthogonal lattice approximating the object shape. Such dipoles belonging to the object $\mathcal{X}$ occupy positions ${}^{\mathcal{X}}\boldsymbol{r} = \boldsymbol{i}d + {}^{\mathcal{X}}\boldsymbol{R_0}$. Components of the 3D index $\boldsymbol{i} = (i_x, i_y, i_z)$ have discrete values equal to $1, 2, \ldots, N$, d denotes the lattice constant and ${}^{\mathcal{X}}\boldsymbol{R_0}$ denotes the position vector of the particle $\mathcal{X}$ in space. The same symbolism is used for the dipole moment ${}^{\mathcal{X}}\boldsymbol{p_i}$ and the incident field ${}^{\mathcal{X}}\boldsymbol{E}_i^{\mathrm{inc}}$ at the place of the dipole $\boldsymbol{i}$ inside the particle $\mathcal{X}$. The total dipole moment ${}^{\mathcal{X}}\boldsymbol{p_i}$ is induced by the final electric field formed from the incident field ${}^{\mathcal{X}}\boldsymbol{E}_i^{\mathrm{inc}}$ and the fields radiated from the dipoles inside the same or other particles:

$$\frac{{}^{\mathcal{X}}\boldsymbol{p}_i}{\alpha} = \sum_j {}^{0}\mathsf{G}_{ij}\,{}^{\mathcal{X}}\boldsymbol{p}_j + \sum_{\mathcal{Y}}\sum_j {}^{\mathcal{X}\mathcal{Y}}\mathsf{G}_{ij}\,{}^{\mathcal{Y}}\boldsymbol{p}_j + {}^{\mathcal{X}}\boldsymbol{E}_i^{\mathrm{inc}}, \tag{3}$$

where α is the polarizability of the dipole [18, 29] and the Green tensors ${}^{0}\mathsf{G}_{ij}$ or ${}^{\mathcal{X}\mathcal{Y}}\mathsf{G}_{ij}$ [18, 24, 29, 30] denote the dipoles inside the same or other particles, respectively. Equation (3) must be solved iteratively to determine all the dipole momenta ${}^{\mathcal{X}}\boldsymbol{p_i}$ in the system. Once they are determined (to a given residual error), the time-averaged total forces acting upon each dipole are calculated [31]:

$$\langle {}^{\mathcal{X}}(F_\xi)_i\rangle = \sum_\nu \tfrac{1}{2}\,\mathrm{Re}\left[{}^{\mathcal{X}}(p_\nu)_i^*\,\partial_\xi({}^{\mathcal{X}}(E_\nu)_i)\right], \quad \text{where } \xi, \nu = \{x, y, z\}. \tag{4}$$

The substantial problem of how to obtain all spatial derivatives of the total electric field ${}^{\mathcal{X}}\boldsymbol{E_i}$ is clarified in [32]. The optical force acting upon the object $\mathcal{X}$ is equal to the sum of the optical forces acting upon all dipoles constituting the object.

The number of dipoles M in configurations described in this paper reaches 1 million. Therefore the convolution method together with fast Fourier transform (FFT) techniques must be used [33]. Because we assume geometrical locations of dipoles on a rectangular lattice, the distance between two arbitrary dipoles $\boldsymbol{r}_{ij}$ depends only on the difference in their indices $\boldsymbol{i}-\boldsymbol{j}$. This is valid also for the dipoles belonging to different objects. Thus $\mathsf{G}_{ij} = \mathsf{G}'_{i-j}$ and the summations in (3) may be converted into convolutions $\sum_j \mathsf{G}_{i-j}\,{}^{\mathcal{X}}\boldsymbol{p}_j$ which are calculated by the FFT. All together these techniques reduce computer memory requirements from M^2 to M and the number of computational steps from M^2 to just $M\ln(M)$ and therefore they significantly speed up the calculation, too.

3. Results

3.1. Optical binding of two particles

Let us first use the CDM method presented in the previous section to calculate the optical forces acting upon two spherical

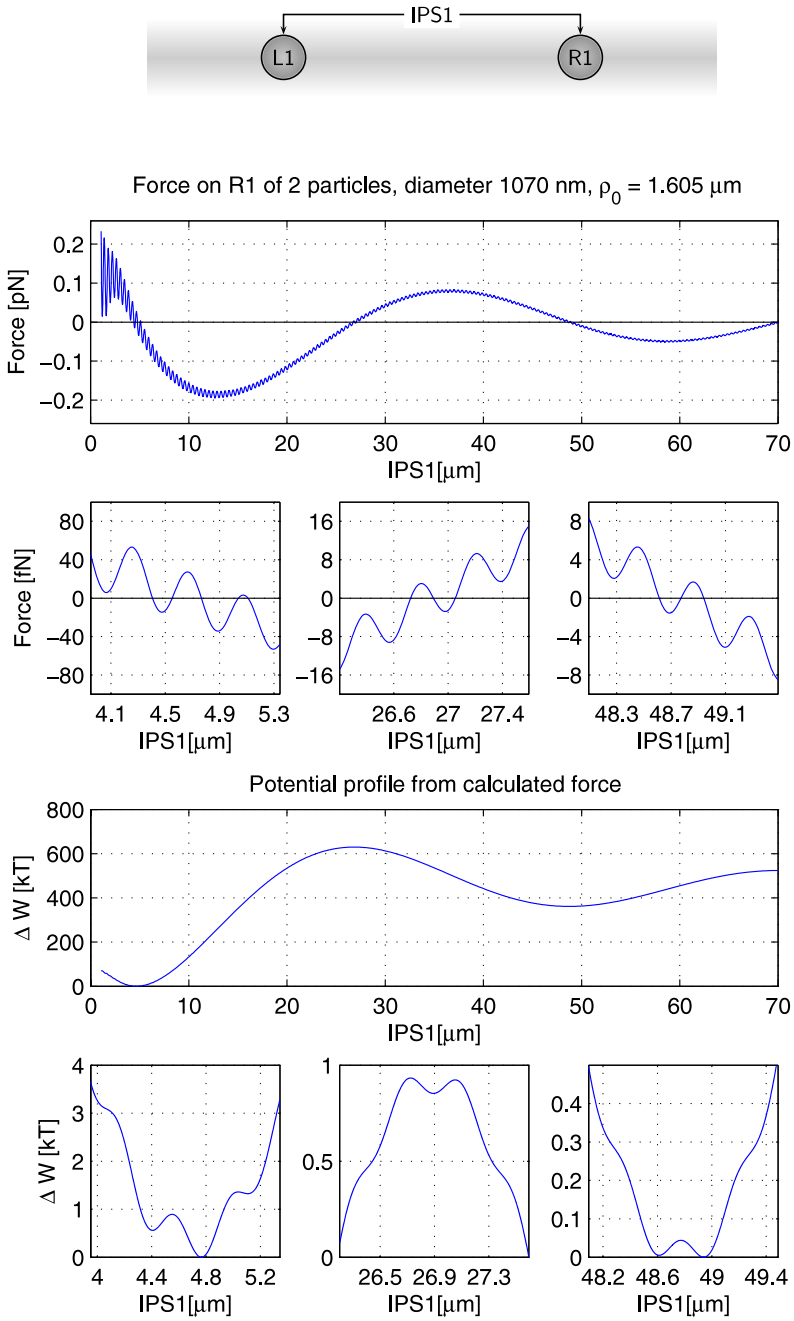

Figure 1. Upper scheme: the arrangement of two identical spherical particles with inter-particle separation IPS1. Upper plots: the longitudinal optical force acting upon the right polystyrene particle R1 as the function of the IPS1. Diameter of the particles is 1070 nm and their refractive index is $n_{sp} = 1.59$. The wavelength of the incident beams is equal to 811 nm and corresponds to D_2O as the surrounding medium. The radius of the Bessel beam core is selected as 1.605 μm. In all figures in this paper we consider the intensity of the optical axis of the single incident Bessel beam equal to 4 mW μm^{-2} which corresponds to the experimental conditions [10]. The equilibrium positions correspond to such IPS1 where the total force is equal to zero and has a negative slope. Three zoomed regions reveal short-period oscillations (amplitude proportional to 1/IPS) giving rise to multiple equilibrium positions (stable sub-configurations) in each region. The evaluation of the mean first passage time (MFPT) [34] at each equilibrium position estimates how long the particles remain there. We found MFPT equal to 0.03 s for IPS1 48.6, 48.9 and 26.9 μm and MFPT equal to 0.1 s for IPS1 4.4 and 4.8 μm.

particles placed on the overlapping optical axis of both counter-propagating mutually incoherent Bessel beams. We assume the particles are localized only at the high intensity centre of the Bessel beam core placed on the optical axis. This is justified by the size of the radial optical force pushing the particle back towards the optical axis if the particle is radially deviated. The maximal value of this force is about 100 times higher than the maximal axial binding force between both particles. The upper part of figure 1 demonstrates how the longitudinal optical binding force depends on the distance between both polystyrene spheres of diameter 1070 nm. The long-period force modulation creates three regions within the studied inter-

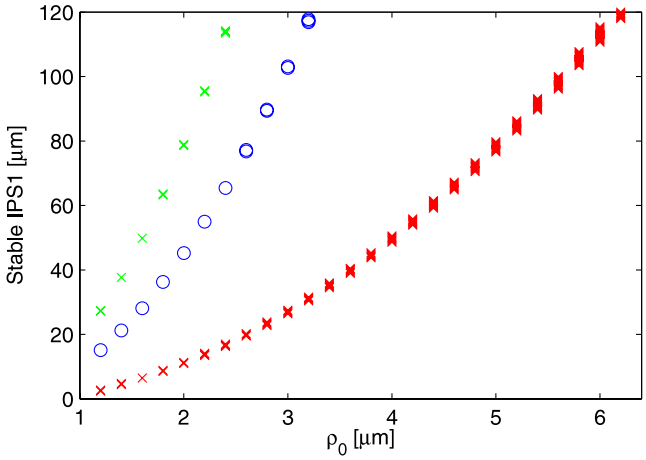

Figure 2. Influence of the radius ρ_0 of the Bessel beam core on the stable inter-particle separations (IPS1) for two 800 nm polystyrene particles immersed in D_2O in the same set-up as in figure 1. Three branches correspond to the three stable regions discussed there. The most stable region with particles closer to each other is denoted by red crosses. The multiple identical marks aligned vertically denote several stable sub-configurations separated by the short-range period. The middle branch (denoted by blue circles) represents, with respect to the thermal activation, the practically unstable central region. The third branch with the largest IPS1 corresponds to the long-range binding in the Bessel beams studied in section 3.4. More than three branches are not studied and shown here.

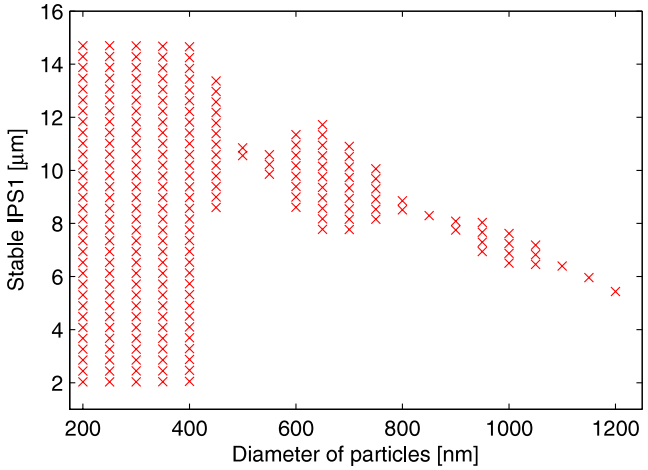

Figure 3. Existence of several stable sub-configurations caused by the amplitude of the short-range force oscillations. Only the stable separations in the range from 2 to 15 μm were considered for the radius of the Bessel beam core $\rho_0 = 1.8$ μm.

particle separation (IPS1) range for which the particles could form stable configurations. The stability factor of each stable configuration depends on the overall shape (envelope) of the optical force and also on the amplitude of the short-range force oscillation. Therefore the first and the third stable configurations for IPS1 around 5 and 49 μm, respectively, form more stable sub-configurations due to the negative slope of the optical force envelope. The second stable configuration with IPS1 around 27 μm is caused by the negative slope of the optical force in the short-range oscillations superimposed on the overall positive force slope. As is demonstrated in the bottom part of figure 1, there exists a stable equilibrium configuration for this IPS1 but, due to the thermal activation, the shallow potential well is fast overcome and the particles approach the first and third stable IPS1 regions mentioned above. There exist two potential minima at these regions but under the studied parameters the mean first passage time from each minimum is shorter than about 0.1 s. Therefore the bound particles frequently change their IPS1 and hop between both potential minima in each region.

The periods of the long-range and short-range modulation of the binding force can be approximated as

$$\frac{2\pi}{k - k_z}\text{—long period,} \qquad \frac{2\pi}{k + k_z}\text{—short period.} \tag{5}$$

The long-range modulation occurs when the field scattered by the object propagates with k in the same direction as the incident Bessel beam with k_z. The short-range modulation comes from the interference of the scattered field counter-propagating with the incident Bessel beam.

Figure 2 demonstrates that the stable IPS1 increases with increasing radius of the Bessel beam core. The number of stable sub-configurations (multiple marks aligned vertically) depends on the particle's diameter—as figure 3 illustrates for the stability branch with the shortest IPS1. As one can also see in figure 3, particles smaller than 400 nm are bound in the whole displayed region of IPS1 between 2 and 15 μm because of the very high amplitude of the short-range oscillations. However, for particles bigger than 400 nm the amplitude of the long-range force oscillations becomes dominant and therefore the stable sub-configurations occur only for some IPS1. It is seen that certain particle diameters do not form several stable sub-configurations and it can be related to the 'size effect' of the particles placed in spatially periodic fields [35, 36]. Figure 3 also demonstrates that the stable IPS1 decreases as the diameter of the particle increases.

Figure 4 compares optical forces acting upon spherical particles of diameters 800 and 1070 nm for different IPS1. The calculated dependence of the optical force on the IPS1 enabled evaluation of the probability density that the particle is found 1 μm from the certain IPS1. These results show that the larger particles are much more localized and three distinct peaks indicate three stable sub-configurations. High sensitivity of the IPS1 and the overall shape of the probability distribution on the radius of the Bessel beam core is shown for three beam radii differing by 30 nm.

3.2. Optical binding of three particles

Firstly we considered a symmetric configuration of identical particles as depicted in the top part of figure 5. The binding forces upon particle R1 and the probability distribution of IPS1 are similar to the case with two optically bound particles (compare figures 4 and 5). However, three particles are placed closer to each other in the stable configurations and the binding force acting upon particle R1 is guided by the convolution of two periodic dependences coming from different distances

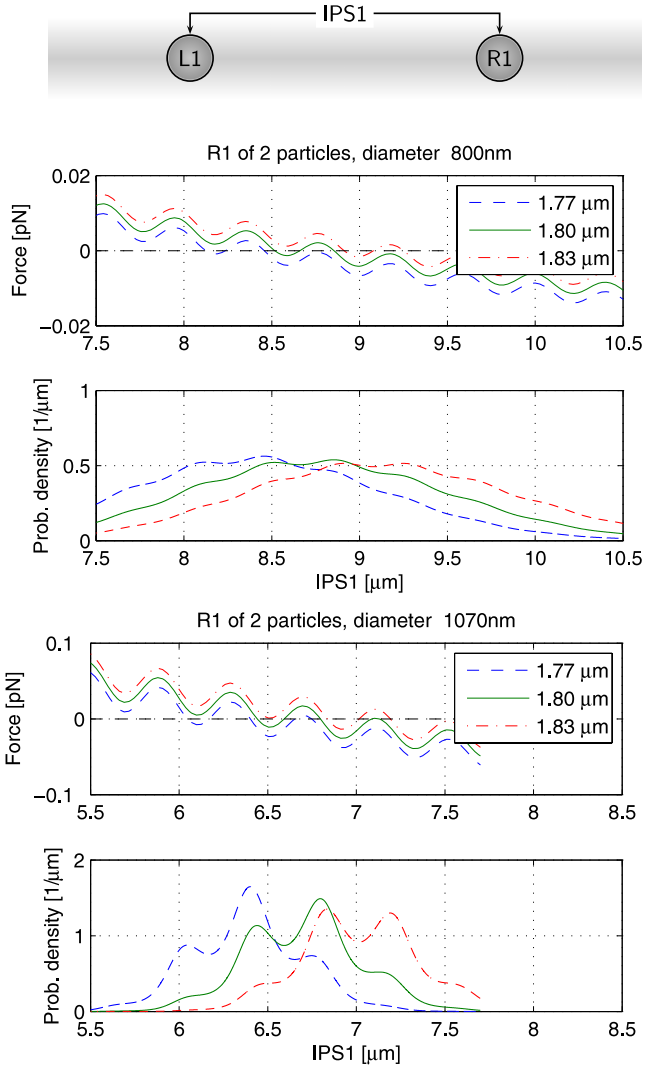

Figure 4. The optical force acting upon particle R1 and the probability distribution of IPS1 is calculated for two identical polystyrene spheres of diameters 800 nm (upper pictures) and 1070 nm (lower pictures). Three values of the Bessel beam core radii $\rho_0 = 1.77$ μm (blue dashed), $\rho_0 = 1.80$ μm (green full) and $\rho_0 = 1.83$ μm (red dashed–dotted) demonstrate high sensitivity of the stable IPS1 and particle behaviour on this parameter.

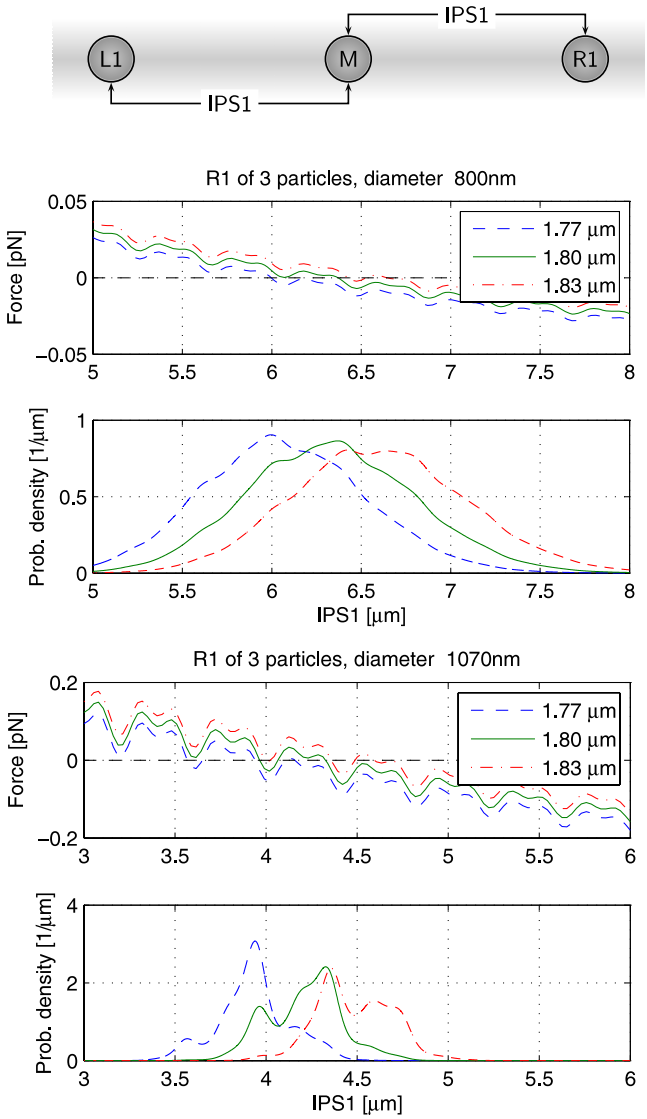

Figure 5. Calculated optical force acting upon the right particle R1 and the IPS1 probability density in a symmetrical configuration of three particles. Parameters of the calculation are the same as in figure 4.

between particle R1 and the other two particles M and L1. Due to the considered symmetrical configuration the force acting upon the middle particle M is equal to zero for all IPS1 and the optical force acting upon the left particle L1 has opposite sign to the force acting upon R1.

We considered also a non-symmetrical arrangement with non-equal inter-particle separations and we looked for new stable configurations of the system. The forces acting upon all three particles are shown in figure 6 as the function of two independent inter-particle separations IPS1 and IPS2. We found four stable configurations, two of them corresponding to the symmetrical arrangement with IPS1 = IPS2 with values 6.1 and 6.4 μm (the particle M is placed in the middle) and the other two corresponding to the mirror image of a non-symmetrical stable configuration with IPS1 = 6.4 μm and IPS2 = 6.1 μm and vice versa.

3.3. Optical binding of four and five particles

In these configurations we considered symmetrical set-ups with two independent inter-particle separations IPS1 and IPS2. The optical forces acting upon 800 nm particles in the configuration with five particles are stronger as the colour bars illustrate in figure 7. Stronger forces result in closer localizations of the particles in stable configurations. From the dependence of the calculated forces on two separation parameters IPS1 and IPS2 we determined their stable combination: IPS1 = 3.6 μm and IPS2 = 4.0 μm. The calculations with four or five 1070 nm particles have not shown any stable binding positions except for the case when all particles are in physical contact. Experimentally it was observed as a collapse of a particle cluster with more than three 1070 nm particles. This type of configuration we do not consider as optically bound.

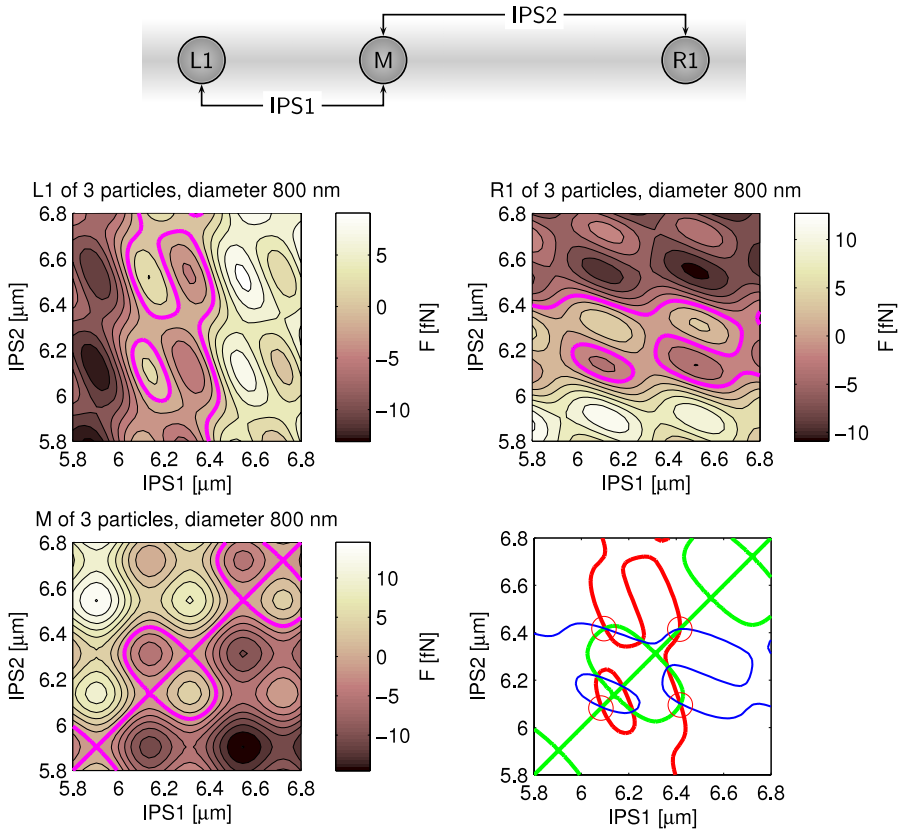

Figure 6. Longitudinal optical forces acting upon all three particles L1, M and R1 if non-symmetrical configurations are also considered (independent IPS1 and IPS2). The particle size is 800 nm and the value of $\rho_0 = 1.80\ \mu$m (compare with figure 5). Purple curves visualize a contour of zero force. Intersections of these zero-force contours denote in the last picture the equilibrium configurations but only those denoted by circles are stable.

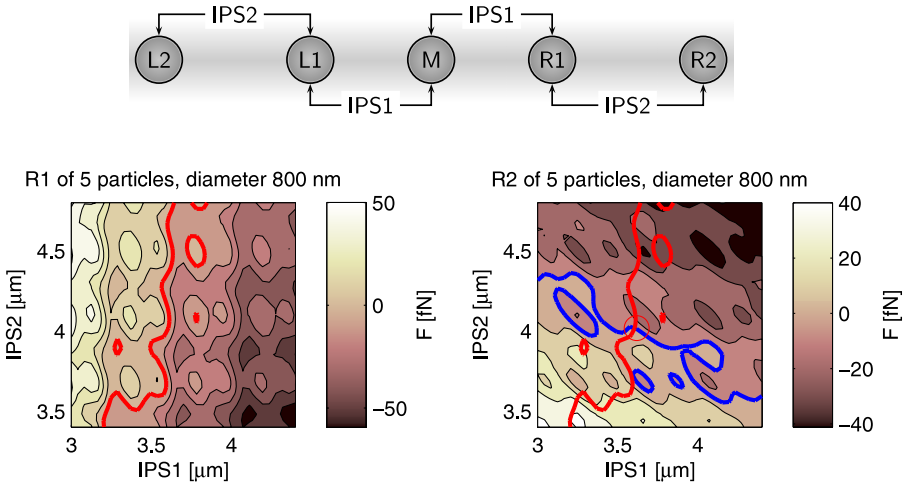

Figure 7. Longitudinal optical forces acting upon particles R1 and R2 in the symmetrical configuration of five particles. We considered two independent inter-particle separations IPS1 and IPS2 (displayed in the top picture). The red (resp. blue) curves show combinations of IPS1 and IPS2 where the force acting upon R1 (resp. R2) is equal to zero. Their stable combination is marked by a red circle. We used the same parameters as in the previous figures and the particle diameter was equal to 800 nm.

3.4. Long-range optical binding in Bessel beams

The long-range modulation of the optical binding force enables stable configurations with particles far from each other (see figures 1 and 2). Assuming the radius of the Bessel beam core equal to 1.8 μm, two particles of diameter 800 nm can settle 63.2 or 63.6 μm far from each other. The CDM enables us to study the configuration of two clusters (see figure 8)

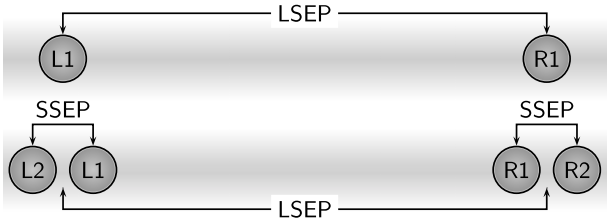

Figure 8. Configurations of particles in the long-range optical binding set-up. Top configuration assumes only two particles separated by long-range separation (LSEP) and it is similar to the set-up in figure 1. Bottom scheme shows two clusters separated by LSEP and each contains two particles separated by short-range separation (SSEP).

separated by long-range separation (LSEP) and each cluster consists of two particles separated by short-range separation (SSEP). Therefore all together four particles are bound in the chain. Stable configurations were found by calculating binding forces for different LSEP and SSEP with the result: LSEP = 64.2 μm, SSEP = 7.6 and 8.0 μm. For comparison the stable IPS1 for two 800 nm particles were 8.5 and 8.8 μm (see figure 4). Therefore the presence of another cluster decreases the separation between two particles in the cluster. However, the presence of two particles in each of the two clusters just weakly modifies the distance between the centres of the clusters compared to the long-range stable configuration of just two bound particles. It seems that the distance between the clusters does not depend substantially on the number of particles in each cluster.

3.5. Comparison with the experiment

We used a low temporal coherence fibre laser working at 1064 nm and providing a maximal output power of 10 W. The output beam was split into two beams with optical path difference 60× larger than the coherence length of the laser, equal to 1 cm, and therefore no interference between both beams occurred. Both beams passed through the axicons to create two counter-propagating Bessel beams. Further demagnifying telescopes decreased the core radii of the Bessel beams. Since the axicon tips were rounded, longitudinal oscillations along the propagation axis occurred. We filtered them off in the back focal plane of the first lens of the demagnifying telescope [37]. The final demagnified radii of the Bessel beam were carefully measured and the following values were obtained: 1.80 ± 0.03, 2.44 ± 0.03 and 3.70 ± 0.02 μm for three different demagnifications of the telescope. The colloidal sample consisted of polystyrene spheres (diameters 800 and 1070 nm) placed in an optical quality cuvette filled with D_2O to suppress any unwanted thermal convection of the fluid due to absorption at the laser wavelength. Positions of the spheres were observed by bright-field illumination and recorded by the fast CCD camera IDT XS-3. Thousands of frames were recorded with various concentrations of particles and number of bound particles in the beams. The individual particle positions were obtained from each frame by a correlation algorithm [38] and the inter-particle separations were analysed. The typical lifetime of observed structures ranged from 10 to 100 s and depended on the concentration of particles in the solution. Usually we observed a gradual increase of the number of particles in the cluster until the cluster collapsed and the particles were in contact. The CDM simulations correspond well to the experimental observations and the results are summarized in table 1. In the majority of cases the theoretical results provide slightly smaller inter-particle separations than we observed experimentally. However, if one takes into account the strong sensitivity of the inter-particle separations on all the parameters of the system—namely the radii of the Bessel beam cores, we consider the agreement as very good. Therefore the CDM can be used to predict the principal behaviour of the optically bound system of spherical particles in a qualitative and quantitative manner.

Table 1. Comparison of inter-particle separations obtained from the CDM calculations and experimental measurements [10]. The following parameters were used: radius of the Bessel beam core $\rho_0 = 1.80 \pm 0.03$ μm, refractive index of D_2O medium 1.320 and diameters 1070 and 800 nm of polystyrene particles ($n_{sp} = 1.59$). The larger and smaller particles did not form stable configurations with more than 4 or 6 particles in the cluster, respectively. In the calculations we assumed mirror symmetry of configurations with 3 and more particles. The spread of the experimental data corresponds to the standard deviation and the theoretical interval reflects the existence of several stable sub-configurations (multistability) for three Bessel beam cores.

No. of part.	IPS1 (μm)	IPS2 (μm)
1070 nm		
2 CDM	6.4–7.2	
2 exp.	6.3 ± 0.3	
3 CDM	4.0–4.6	
3 exp.	3.4 ± 0.5	
800 nm		
2 CDM	8.5–9.3	
2 exp.	8.9 ± 0.3	
3 CDM	6.1–6.7	
3 exp.	5.7 ± 0.3	
4 CDM	4.4–4.5	4.8–5.2
4 exp.	4.2 ± 0.5	4.8 ± 0.3
5 CDM	3.6	4.0
5 exp.	3.2 ± 0.2	4.1 ± 0.2

Figure 9 compares the long-range stable configurations of particles in all studied radii of the Bessel beams. It is seen that the distance between the clusters and also the maximum number of particles in each cluster strongly depend on the radii of the Bessel beams. The wider the Bessel beam core, the greater the distance between the clusters and the larger number of particles in each cluster.

4. Conclusions

In this paper we demonstrated successful use of the coupled dipole method (CDM) to predict the stable configurations of longitudinally bound spherical particles. We considered a geometry of two counter-propagating mutually incoherent Bessel beams to suppress the influence of the longitudinal beam intensity variation on the optical binding. We studied the influence of the particle diameters and the radius of the Bessel

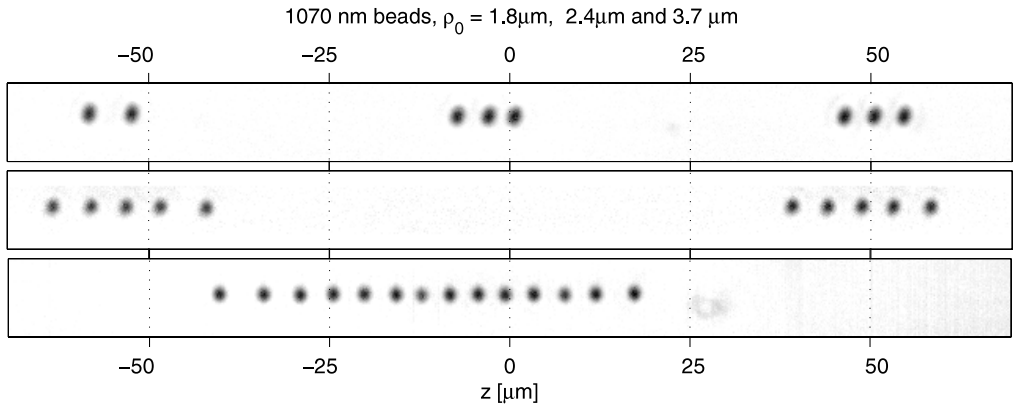

Figure 9. The chains formed by particles of diameter equal to 1070 nm placed in the Bessel beams of three different core radii 1.80 ± 0.03, 2.44 ± 0.03 and 3.70 ± 0.02 μm, corresponding to the pictures going from the top to the bottom. The average distance between the clusters demonstrates the effects of the forward-scattered radiation and it can be approximated by the analytical formula for the long-range period (5). Larger radii of the Bessel beam cores generally lead to higher numbers of particles in each individual cluster and also to larger separations between the clusters. Because of the limited camera field of view the neighbouring clusters are not displayed for the widest Bessel beam.

beam core on the inter-particle separations for two, three, four and five optically bound particles. High sensitivity of the inter-particle separations and number of stable configurations on these parameters was observed. We found that increasing the number of bound particles decreases the inter-particle separation and increases the binding optical force acting upon individual particles. Configurations with three particles can form non-symmetrical stable arrangements. Stable clusters with four and five particles are arranged so that inter-particle separations between outer particles are larger comparing to the inner ones. We also studied theoretically the stable long-range configurations with two clusters composed of two particles because these arrangements were observed experimentally. Theoretical CDM predictions were compared with quantitative experimental observations for different numbers of particles and radii of the Bessel beam cores. It proved that the CDM is the appropriate tool to study multi-particle self-arrangements in laser beams and can be further extended to non-spherical particles, too.

Acknowledgments

The authors appreciated the valuable comments of M Šiler. This work was partially supported by the ISI IRP (AV0Z20650511) and MEYS CR (LC06007, OC08034).

References

[1] Burns M M, Fournier J M and Golovchenko J A 1989 *Phys. Rev. Lett.* **63** 1233–6
[2] Burns M M, Fournier J M and Golovchenko J A 1990 *Science* **249** 749
[3] Mohanty S K, Andrews J T and Gupta P K 2004 *Opt. Express* **12** 2749–56
[4] Tatarkova S A, Carruthers A E and Dholakia K 2002 *Phys. Rev. Lett.* **89** 283901
[5] Singer W, Frick M, Bernet S and Ritsch-Marte M 2003 *J. Opt. Soc. Am.* B **20** 1568–74
[6] Metzger N K, Dholakia K and Wright E M 2006 *Phys. Rev. Lett.* **96** 068102
[7] Metzger N K, Wright E M and Dholakia K 2006 *New J. Phys.* **8** 139
[8] Metzger N K, Wright E M, Sibbett W and Dholakia K 2006 *Opt. Express* **14** 3677–87
[9] Mellor C D and Bain C D 2006 *Chem. Phys. Chem.* **7** 329–32
[10] Karásek V, Čižmár T, Brzobohatý O, Zemánek P, Garcés-Chávez V and Dholakia K 2008 *Phys. Rev. Lett.* **101** 143601
[11] Depasse F and Vigoureux J M 1994 *J. Phys. D: Appl. Phys.* **27** 914–9
[12] Nieto-Vesperinas N, Chaumet P C and Rahmani R 2004 *Phil. Trans. R. Soc.* A **362** 719
[13] Andrews D L and Bradshaw D S 2005 *Opt. Lett.* **30** 783–5
[14] Bradshaw D S and Andrews D L 2005 *Phys. Rev.* A **72** 033816
[15] Bradshaw D S and Andrews D L 2006 *Phys. Rev.* A **73** 039903
[16] Bradshaw D S and Andrews D L 2005 *Opt. Lett.* **30** 3039–41
[17] Guillon M 2006 *Opt. Express* **14** 3045–55
[18] Karásek V and Zemánek P 2007 *J. Opt. A: Pure Appl. Opt.* **9** S215–20
[19] Ng J, Lin Z F, Chan C T and Sheng P 2005 *Phys. Rev.* B **72** 085130
[20] Grzegorczyk T M, Kemp B A and Kong J A 2006 *J. Opt. Soc. Am.* A **23** 2324–30
[21] Taylor J M, Wong L Y, Bain C D and Love G D 2008 *Opt. Express* **16** 6921–8
[22] Chaumet P C and Nieto-Vesperinas M 2000 *Phys. Rev.* B **61** 14119–27
[23] Chaumet P C and Nieto-Vesperinas M 2001 *Phys. Rev.* B **64** 035422
[24] Karásek V, Dholakia K and Zemánek P 2006 *Appl. Phys.* B **84** 149–56
[25] Jarutis V, Paškauskas R and Stabinis A 2000 *Opt. Commun.* **184** 105–12
[26] Čižmár T 2006 Optical traps generated by non-traditional beams *PhD Thesis* Masaryk University in Brno http://www.isibrno.cz/omitec/download.php?Cizmar_hD_thesis.pdf
[27] Durnin J, Miceli J J and Eberly J 1987 *Phys. Rev. Lett.* **58** 1499–501
[28] Čižmár T, Šiler M and Zemánek P 2006 *Appl. Phys.* B **84** 197–203
[29] Draine B 1988 *Astrophys. J.* **333** 848–72
[30] Jackson J D 1999 *Classical Electrodynamics* (New York: Wiley)
[31] Chaumet P and Nieto-Vesperinas M 2000 *Opt. Lett.* **25** 1065–7
[32] Hoekstra A G, Frijlink M, Waters L B F M and Sloot P M A 2001 *J. Opt. Soc. Am.* A **18** 1944–53

[33] Draine B T and Flatau P J 1994 *J. Opt. Soc. Am.* A **11** 1491–9
[34] Gardiner C W 2004 *Handbook of Stochastic Methods* (Berlin: Springer)
[35] Zemánek P, Jonáš A and Liška M 2002 *J. Opt. Soc. Am.* A **19** 1025–34
[36] Čižmár T, Garcés-Chávez V, Dholakia K and Zemánek P 2005 *Appl. Phys. Lett.* **86** 174101
[37] Brzobohatý O, Čižmár T and Zemánek P 2008 *Opt. Express* **16** 12688–700
[38] Cheezum M K, Walker W F and Guilford W H 2001 *Biophys. J.* **81** 2378–88